Transfer of spin angular momentum from Cs vapor to nearby Cs salts through laser-induced spin currents

K. Ishikawa
Graduate School of Material Science, University of Hyogo, Ako-gun, Hyogo 678-1297, Japan

B. Patton,* B. A. Olsen, Y.-Y. Jau,† and W. Happer
Joseph Henry Laboratory, Department of Physics, Princeton University, Princeton, New Jersey 08544, USA
(Received 25 April 2011; published 14 June 2011)

Optical pumping of alkali-metal atoms in vapor cells causes spin currents to flow to the cell walls where excess angular momentum accumulates in the wall nuclei. Experiments reported here indicate that the substantial enhancement of the nuclear-spin polarization of salts at the cell walls is primarily due to the nuclear-spin current, with a lesser contribution from the electron-spin current of the vapor.

DOI: 10.1103/PhysRevA.83.063410 PACS number(s): 32.80.Xx, 32.30.Dx, 34.35.+a, 76.60.−k

I. INTRODUCTION

This paper presents details on a method for increasing the sensitivity of nuclear magnetic resonance (NMR) and other experiments by hyperpolarizing the target nuclei. Hyperpolarized nuclei, that is, nuclear-spin polarizations much larger than the thermal-equilibrium values, can be produced in a variety of materials. For example, molecular solutions [1], amorphous silicon [2], GaAs [3], molecular crystals [4], and ionic crystals [5] have all been hyperpolarized by dynamic nuclear polarization—with or without optical excitation. Other polarization methods include spin exchange between optically pumped alkali-metal atoms and noble gases [6] or chemical reaction products [7] in the gas phase, spin transfer at solid surfaces from hyperpolarized noble gases [8], and chemical synthesis with para-hydrogen [9].

Alkali salts are candidates for accumulating and storing spin polarization. Nuclei with $I > 1/2$ will, in general, depolarize quickly due to quadrupole relaxation. However, ^{133}Cs ($I = 7/2$), ^{7}Li ($I = 3/2$), and ^{6}Li ($I = 1$) all have small quadrupole moments, and thus greatly reduced quadrupole relaxation. Compared to $T_1 = 0.25$ s of ^{87}Rb in RbCl [10], the spin relaxation times of these isotopes at room temperature are very long, for example, 300 s for ^{133}Cs in CsH, 1000 s for ^{133}Cs in CsCl, 900 s for ^{2}H ($I = 1$) in CsD, and 9000 s for ^{1}H ($I = 1/2$) in CsH [11]. See Ref. [12] for other nuclei in alkali salts.

In this work, we report on experimental and theoretical studies of the transfer of spin angular momentum from optically pumped alkali-metal atoms to materials on the inner walls of the container of the vapor. No mediation by other substances, such as noble gases, is needed. Optically polarized atoms transport the angular momentum of the electron and nuclear spins to the cell walls either by diffusion through a buffer gas like nitrogen or by free flight in vacuum. The electron- and nuclear-spin polarizations can be exchanged or lost to translational angular momentum by collisions with buffer-gas atoms or molecules, collisions with other alkali-metal atoms, and collisions with the wall. Experiments of this type were recently reported by Ishikawa *et al.*, who demonstrated high-field optical pumping of Cs vapor and spin transfer from the vapor to CsH salt at 9.4 T [13], as shown in Fig. 1. This result suggests that the angular momentum of the laser photons is transferred to the nuclei of the solid. Experiments have shown that the nuclear polarization enhancement only occurs when the laser is tuned to an optical transition within the atomic vapor. From these results, we conclude that the spin transfer process is mediated by polarization of vapor-phase atoms, since direct optical pumping of the salt or F centers would likely exhibit a very broad optical frequency dependence.

Though these observations show that light absorption by the vapor leads to hyperpolarization of the salt, they do not reveal the mechanism of spin transfer from the vapor to the salt. As described in the remainder of this paper, we measured Cs NMR enhancement under a range of experimental conditions: we varied the laser frequency and polarization, the vapor cell temperature, the buffer-gas pressure, and the externally applied magnetic field; we also performed measurements on a large number of alkali vapor and salt cells. We analyze the results of these measurements with theoretical models of the nuclear- and electron-spin currents through the alkali vapor to the cell walls. One clear conclusion from these studies is that most of the observed enhancement of the nuclear-spin polarization in the walls comes from the current of nuclear-spin polarization through the vapor, with the electron-spin polarization current playing a much smaller role.

II. LASER-INDUCED SPIN CURRENTS

In this section, we describe the theoretical background for spin currents induced by optical pumping. Since this paper is focused on experimental results, we will only outline the theory used to interpret the experiments, and we will refer the reader to the recent book, *Optically Pumped Atoms* [14], for more details.

Figure 2 shows the energy levels of Cs atoms in a high magnetic field. Since the Zeeman splitting, $\hbar\omega_S$, is much larger than hyperfine splittings, $A(I + 1/2)$, the energy eigenstates, $|\mu\rangle$, differ little from the Kronecker product of electron

*Present address: Department of Physics, University of California, Berkeley, CA 94720.

†Present address: Sandia National Laboratories, Albuquerque, NM 87185-1082.

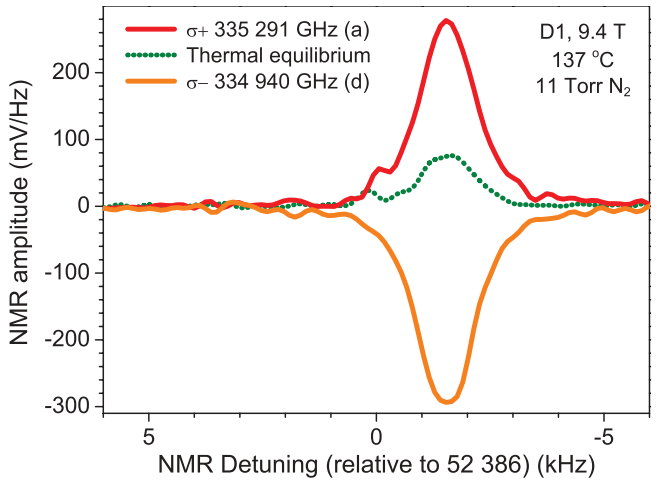

FIG. 1. (Color online) Cs NMR spectra of CsH with 11 Torr N_2, enhanced by optical pumping of Cs vapor. The positive (red line) and negative (orange line) traces show the enhancement from thermal equilibrium (dotted green line) by σ_+ and σ_- light, respectively. The σ_+ and σ_- D_1 transitions ($6p\,^2P_{1/2} - 6s\,^2S_{1/2}$) are 350 GHz detuned from each other due to the Zeeman splitting at 9.4 T. (a) and (d) refer to the D_1 pumping transitions shown in Fig. 2. NMR detuning is relative to 52.386 MHz.

and nuclear-spin states, $|I\,m_I\rangle \otimes |S\,m_S\rangle$ for the ground state, and similarly $|I\,m_I\rangle \otimes |J\,m_J\rangle$ for the excited state. We will therefore denote the energy states by $|\mu\rangle = |m_S,m_I\rangle$ with $|m_S,m_I\rangle \approx |Im_I\rangle \otimes |Sm_S\rangle$, and with analogous notation for excited atoms. In a glass cell with sufficient buffer gas such that the mean free path of an atom is much smaller than the characteristic dimension d of the cell, optically pumped alkali atoms can transport angular momentum by diffusion through

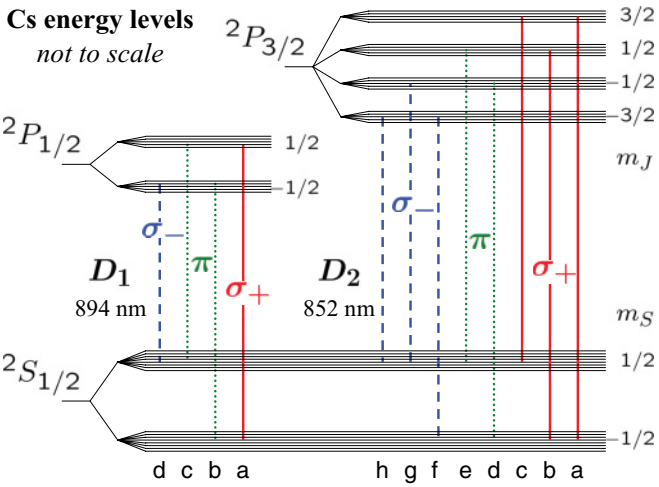

FIG. 2. (Color online) Energy levels of Cs atoms at high magnetic field. The electronic angular momentum projection m_S (m_J) for the ground (excited) state is indicated by a half-integer. There are eight nuclear-spin levels $|I = 7/2\,m_I\rangle$ in each electronic level. The vertical lines denote groups of high-field, allowed, and forbidden D_1 and D_2 transitions, labeled from right to left in order of decreasing resonance frequency [D_2(a-h), D_1(a-d)]. The most effective photon polarization for each transition is indicated by the type of lines: solid red (σ_+), dotted green (π), and dashed blue (σ_-).

the gas to the cell walls. The atoms gain angular momentum through optical excitation and subsequent deexcitation [15]. The excited-state atoms undergo collisional relaxation before repopulating the ground state through spontaneous radiative decay or quenching. The ground-state atoms experience a large number of collisions with the buffer gas that induce spin-rotation and hyperfine-shift interactions, and collisions with other alkali atoms that induce spin-exchange interactions; the electron- and nuclear-spin polarizations couple to each other through all of these collisions. Angular momentum transport to the walls is discussed using the expectation value of the longitudinal electron spin $\langle S_z\rangle$ and the nuclear spin $\langle I_z\rangle$ (in units of $\hbar$) [13]. We describe the evolution of the ground-state density matrix $|\rho\rangle$, represented as a column vector in Liouville space, with the evolution equation [16]

$$\frac{\partial}{\partial t}|\rho\rangle = D\nabla^2|\rho\rangle - G|\rho\rangle\,. \tag{1}$$

We assume that the dependence of the diffusion coefficient D on the number density $[N]$ of the buffer gas and the absolute temperature T of the gas can be adequately parameterized as

$$D = D_0\frac{[N_0]\sqrt{T}}{[N]\sqrt{T_0}}. \tag{2}$$

Here D_0 is the value of the diffusion coefficient at a reference temperature T_0, and at a reference number density $[N_0]$, often taken to be one amagat or the number density of an ideal gas at a pressure of 1 atm and a temperature of 0 °C ($[N_0] = 2.69 \times 10^{19}\text{cm}^{-3}$). For nitrogen gas, Beverini *et al.* [17] report $D_0 = 0.087$ cm^2 s^{-1} for $T_0 = 290$ K.

The second term on the right-hand side of Eq. (1), $-G|\rho\rangle$, describes the evolution of the density matrix that is independent of spatial diffusion. The operator G is represented by a square matrix in Liouville space [14,18]. We write $G|\rho\rangle$ as a sum of contributions due to different mechanisms: hyperfine couplings within the atom, coupling to externally applied magnetic fields, optical pumping as $|\dot\rho_{\rm dp}\rangle$ from depopulation pumping and $|\dot\rho_{\rm rp}\rangle$ from repopulation pumping, and collisional relaxation processes as $|\dot\rho_{\rm sd}\rangle$ from the spin-rotation interaction and $|\dot\rho_{\rm hs}\rangle$ from the hyperfine-shift interaction [14,19]. The repopulation rate, $|\dot\rho_{\rm rp}\rangle$, is the sum of a contribution $|\dot\rho_{\rm q}\rangle$ due to quenching of excited atoms by collisions with nitrogen molecules and a contribution $|\dot\rho_{\rm sp}\rangle$ for spontaneous decay. We ignore collisional depolarization of the excited state, as distinct from quenching collisions, and we also ignore radiation trapping for the moment. We assume that G is spatially uniform—the laser is so intense that the top-hat beam passes through the atomic vapor without any change in shape or intensity, and collisions in the vapor are homogeneous.

Collisions with buffer-gas atoms or molecules cause transitions between the energy sublevels of the atom. For the atomic ground state, the most important collisional interactions are as follows:

(1) The spin-rotation interaction $\gamma\,\mathbf{N}\cdot\mathbf{S}$ between the rotational angular momentum $\mathbf{N}$ of the colliding pair and the electron spin $\mathbf{S}$ of the alkali-metal atom. This interaction leads to S damping at the characteristic rate $\Gamma_{\rm sd} = \kappa_{\rm sd}[N]$ [17] with $\kappa_{\rm sd} = 820\ \text{s}^{-1}\text{amg}^{-1}$.

(2) The collisional hyperfine-shift interaction $\delta A\,\mathbf{I}\cdot\mathbf{S}$ between the nuclear spin $\mathbf{I}$ of the alkali-metal atom and the

electron spin **S**. This interaction leads to transitions at the characteristic rate $\Gamma_{\rm hs} = \kappa_{\rm hs}[N]$ [20,21] with $\kappa_{\rm hs} = 55\ {\rm s}^{-1}{\rm amg}^{-1}$.

The spin-exchange interaction—the largest term is field-dependent—changes $\langle I_z\rangle$ with the rate $2\delta^2\Gamma_{\rm se}$ [22] where $\delta = A/2\hbar\omega_S$ is small at a high field, $\Gamma_{\rm se} \propto [{\rm Cs}]$ is the spin-exchange rate at the low fields, and [Cs] is the number density of Cs atoms. For the experiments described here, the number density [Cs] is no larger than the saturated vapor pressure of the condensed solid or liquid alkali metal in the cell. The measured density can be a factor of two or more smaller than this equilibrium limit because of loss of alkali-metal atoms into the glass walls. For most of these experiments the temperatures were low enough ($T \lesssim 100\ ^\circ$C) and the associated number densities of Cs atoms were small enough to neglect the rate of spin-exchange collisions between pairs of Cs atoms, in comparison to the rates $\Gamma_{\rm sd}$ and $\Gamma_{\rm hs}$ mentioned above.

We assume that atoms impinging on the uncoated glass walls are adsorbed, and that the adsorbed atoms are replaced by unpolarized, desorbed atoms. We ignore the extremely small equilibrium spin polarization, since the thermal energy $k_{\rm B}T$ is so large compared to the energy differences between spin sublevels, $|\mu\rangle$. We also ignore the small corrections to this boundary condition due to the finite mean free path of the diffusing atoms and the possibility that the atoms may bounce off the wall with some of their precollision polarization intact [14,23]. Then the density matrix of the atoms at the walls is very nearly given by

$$\rho_{\rm w} = \frac{1}{[I][S]}\sum_{\mu}|\mu\rangle\langle\mu|. \tag{3}$$

Here $[I] = 2I + 1$ is the number of nuclear-spin sublevels, and $[S] = 2S + 1 = 2$ is the number of electron-spin sublevels. The boundary condition (3) is well justified for the experiments reported here, where the nuclear polarization of atoms desorbing from the walls is negligibly small, but Eq. (3) could be modified to account for the larger nuclear polarizations that we hope will be produced in the future. Equation (3) implies that the longitudinal electronic spin $\langle S_z\rangle_{\rm w}$ and nuclear spin $\langle I_z\rangle_{\rm w}$ both vanish at the walls, that is,

$$\langle S_z\rangle_{\rm w} = 0 \quad \text{and} \quad \langle I_z\rangle_{\rm w} = 0. \tag{4}$$

Near the walls, the vapor has a large specific absorption, leading to bright, easily observed fluorescence [12].

When an unpolarized atom is desorbed from the cell wall and begins to diffuse into the interior, it will begin to be polarized under the combined effects of optical pumping and collisional spin relaxation. Since an atom can diffuse a distance of order $\sqrt{D\tau}$ through the buffer gas in a time τ, we see that the characteristic distance of diffusion needed to equilibrate the populations of spin sublevels is $\sqrt{D/\Gamma_{\rm sd}} = 0.93$ cm for the spin-rotation interaction and $\sqrt{D/\Gamma_{\rm hs}} = 3.6$ cm for the hyperfine-shift interaction. These lengths are on the order of the cell size, so we expect the spin polarization to be nonuniform throughout the cell volume, with the highest polarizations at locations farthest from the walls.

At high magnetic fields, the hyperfine-shift interaction $\delta A\,\mathbf{I}\cdot\mathbf{S}$, acting during a collision, drives transitions, satisfying the selection rule $\Delta m_I = -\Delta m_S$ between ground-state sublevels. Thus, the collisional hyperfine-shift interaction tends to equalize the populations of sublevels with the same total azimuthal quantum number $m = m_S + m_I$, and it causes part of the electron spin (produced by optical pumping) to be transferred to the nuclear spin or vice versa, making up the heart of hyperfine-shift pumping. The spin-rotation interaction $\gamma\,\mathbf{N}\cdot\mathbf{S}$, acting during a collision, drives transitions between ground-state sublevels satisfying the selection rule $\Delta m_I = 0$. The spin-rotation interaction cannot directly affect the nuclear polarization of the atoms, and this means that polarization modes with mostly nuclear-spin polarization and little electron-spin polarization take a long time to build up to equilibrium and they have small amplitudes in cells that contain little buffer gas.

Assuming cylindrical symmetry about the beam axis (parallel to the magnetic field), the radial current densities of longitudinal electronic and nuclear spin are

$$J_S = -[{\rm Cs}]D\frac{\partial\langle S_z\rangle}{\partial r} \quad \text{and} \quad J_I = -[{\rm Cs}]D\frac{\partial\langle I_z\rangle}{\partial r}, \tag{5}$$

where r is the radial coordinate. In our model, we use the boundary condition (3) to numerically solve the evolution

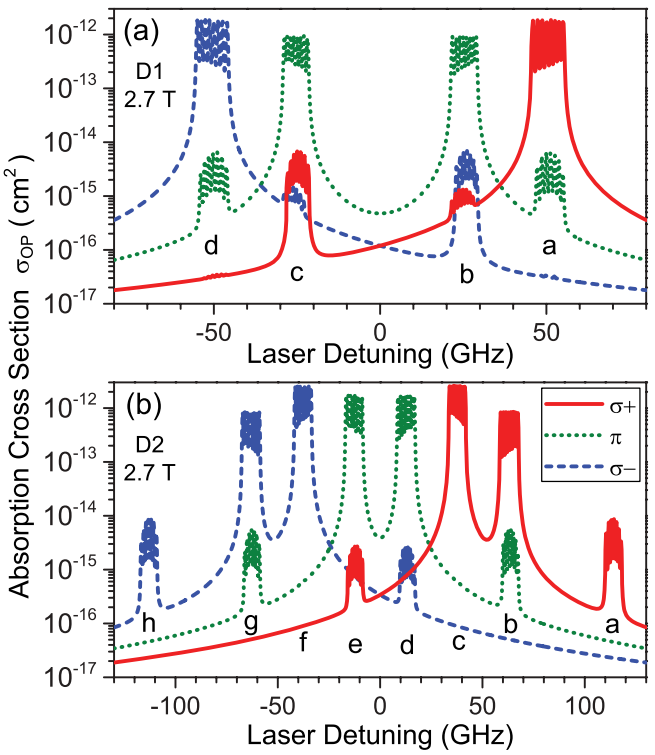

FIG. 3. (Color online) Absorption cross section of Cs atoms for σ_+ (solid red line), π (dotted green line), and σ_- (dashed blue line) light for (a) D_1 line and (b) D_2 line at 2.7 T and 10 Torr of N_2 gas. The horizontal axis is the detuning of single-mode laser from the resonance frequency of hypothetical atoms ($I = 0$) with no magnetic field. Lowercase letters denote the transition frequencies noted in Fig. 2. Cross sections on resonance for transitions with $\Delta m_I = \pm 1$ are roughly three orders of magnitude smaller than those for transitions with $\Delta m_I = 0$, and smaller by additional orders of magnitude for $\Delta m_I = \pm 2$. Note the logarithmic vertical scale. The absorption length can be calculated from the cross section and the number density [Cs] = $1.5 \times 10^{13}{\rm cm}^{-3}$ (100 °C).

equation (1) in Liouville space with linear algebra techniques [14]. We use the resulting steady-state density matrix, $|\rho)$, to evaluate spatially dependent values of $\langle S_z\rangle = \mathrm{Tr}[\rho S_z]$ and $\langle I_z\rangle = \mathrm{Tr}[\rho I_z]$, and we numerically evaluate the derivatives at the cell walls to find the currents (5). Comparing observed enhancements to simulated spin currents should yield insight into the vapor-solid spin transfer mechanism.

Fully allowed optical transitions have the selection rules, $\Delta m_I = 0$. The fully allowed D_1 transitions are $|m_S = \mp 1/2, m_I\rangle \leftrightarrow |m_J = \pm 1/2, m_I\rangle$ for $\sigma_\pm$-polarized light and $|m_S = \pm 1/2, m_I\rangle \leftrightarrow |m_J = \pm 1/2, m_I\rangle$ for π-polarized light. Although the high-field energy eigenstates are nearly pure product states, the hyperfine interaction will cause a slight admixture of product states with the same azimuthal quantum number $m = m_S + m_I$. For example, the energy eigenstate $|m_S, m_I\rangle$ will have slight admixtures of the product states, $|I\, m_I'\rangle \otimes |S\, m_S'\rangle$ with $m_S' \neq m_S$ and $m_I' \neq m_I$ but with $m_S' + m_I' = m_S + m_I$. There will be analogous mixing of excited-state sublevels. This makes it possible for optical excitation to drive weaker, "forbidden" transitions (see Fig. 3) with $\Delta m_I \neq 0$. At the frequencies of transitions D_1(b), $|m_S = -1/2\rangle \leftrightarrow |m_J = -1/2\rangle$, the atoms can be excited weakly by $\sigma_\pm$ light ($\Delta m_I = \pm 1$) and strongly by π light ($\Delta m_I = 0$). The electron spin $\langle S_z\rangle$ produced by all three polarizations of light is positive at the transitions D_1(b), since the sublevels with $m_S = -1/2$ are depopulated for all three polarizations, as shown in Fig. 4. On the other hand, the nuclear spin $\langle I_z\rangle$ produced by the optical pumping depends strongly on the light polarization, since pumping with "forbidden" transitions can increase or decrease m_I directly.

From numerical solutions of Eq. (1), we calculate J_S and J_I at several magnetic fields for all polarizations of light. The pump frequency dependence of these currents is shown in Figs. 5–7, for pump light power density $P_L = 100$ mW/cm^2, N_2 gas pressure of 10 Torr, and temperature 100 °C. The current J_S depends on pump power as $\sqrt{P_L}$ when the pumping rate Γ_{op} is much larger than Γ_{sd} and Γ_{hs} [13]. As shown in

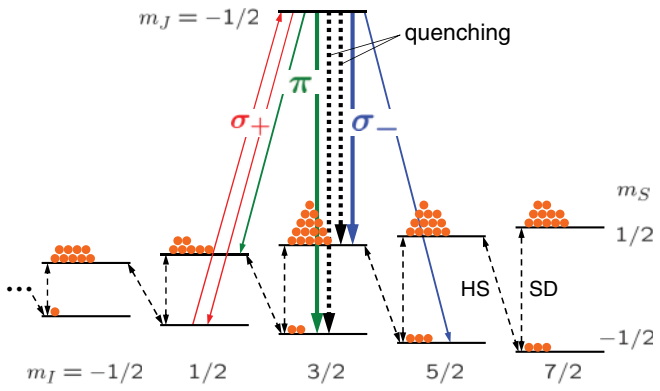

FIG. 4. (Color online) Spin sublevel population is represented as orange (gray) beads for σ_+ pumping at D_1(b). The solid arrows indicate optical excitation and spontaneous decays. The dotted arrows indicate quenching, S-damping (SD), and hyperfine-shift (HS) collisions. Since a single-mode laser pumps the adjacent nuclear-spin levels, the electron spin is well polarized by depopulation pumping. The nuclear polarization is due to hyperfine-shift pumping and the $\Delta m_I = 1$ transition by σ_+ light.

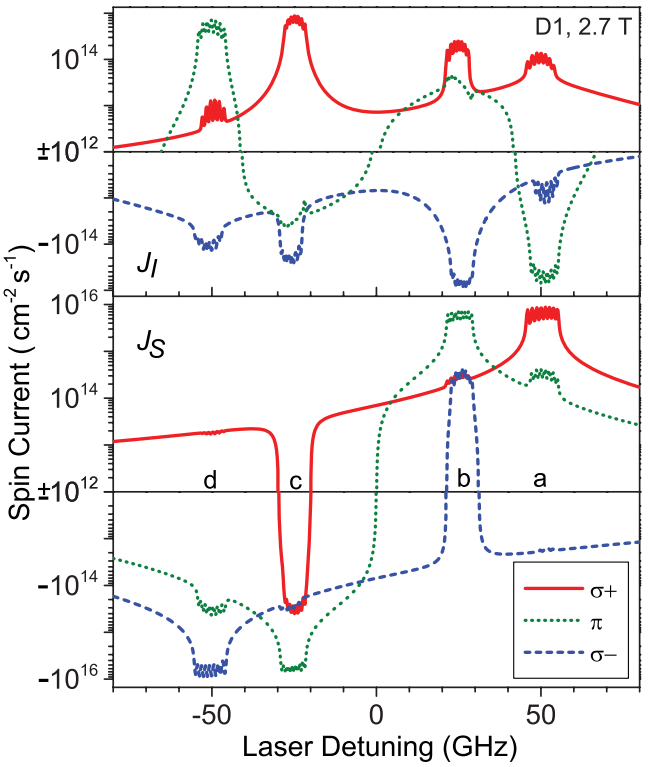

FIG. 5. (Color online) Simulated diffusion spin currents to the side wall of a cylindrical cell (inner diameter 1 cm) at a magnetic field of 2.7 T as a function of laser pumping frequency detuning from the center of the D_1 line. Nuclear- and electron-spin currents J_I and J_S are induced by σ_+ (solid red line), π (dotted green line), and σ_- (dashed blue line) light. All were calculated at 100 °C with 10 Torr N_2 and uniform laser power density of 100 mW/cm^2. The logarithmic scale for both positive and negative spin currents makes the curves discontinuous when the current changes sign. Lowercase letters indicate the transitions noted in Fig. 2. It is important to notice that for each of the transitions a, b, c and d, the nuclear-spin current J_I has the same sign for the same circular polarization and the current reverses sign when the sign of the circular polarization is reversed.

Fig. 5, a large positive electron-spin current is induced by σ_+ pumping (solid red curve) with the D_1(a) line, and this feature shows a broad Lorentzian tail. The broad tail of J_I near the D_1(a) transition comes from coupling to J_S through hyperfine-shift pumping. The four peaks in J_I are due to optical pumping, and the largest current is induced at D_1(c), not at the allowed transition D_1(a). For transition D_1(c), J_S is negative for any light polarization, and J_I is positive only for σ_+ light. Similarly, the only negative spin current for D_1(b) is J_I induced by σ_- pumping. The nuclear-spin current to the walls will play a key role in studying spin transfer to salts.

The currents J_S and J_I are induced in a variety of combinations from D_2(a) through D_2(h) at 2.7 T, as shown in Fig. 6. Note that the D_2(a) and D_2(h) lines would be forbidden transitions at infinite magnetic field ($m_J = m_S \pm 2$, $\Delta m_I = \mp 1$). At D_2(a), σ_+ pumping induces $J_S > 0$ and $J_I < 0$, and other light polarizations produce no resonant spin currents. Pumping with σ_- light at D_2(h) induces $J_S < 0$ and $J_I > 0$. The relatively simple behavior of the vapor undergoing pumping at one of these transitions will be useful for studying

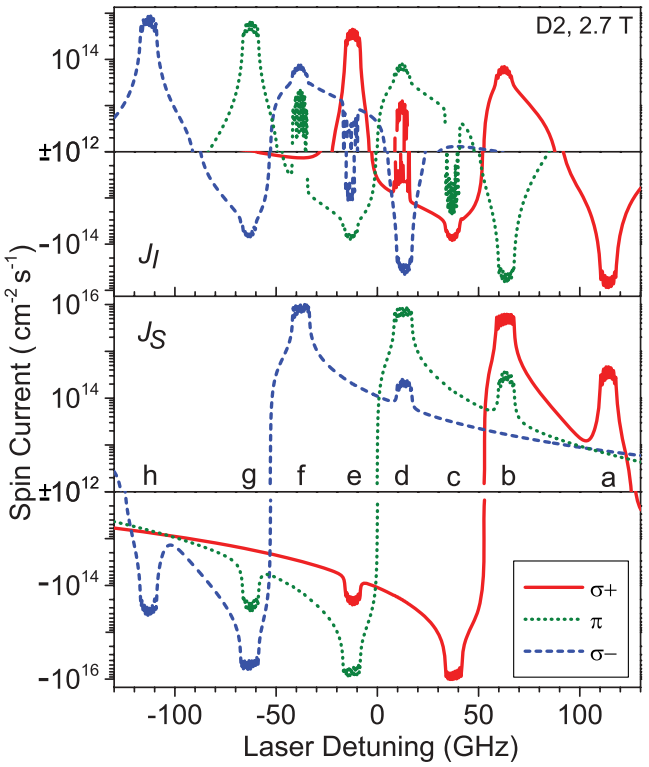

FIG. 6. (Color online) Simulated diffusion spin currents to the side wall of a cylindrical cell as a function of laser frequency across the D_2 line at 2.7 T. Nuclear- and electron-spin currents, J_I and J_S, are induced by σ_+ (solid red line), π (dotted green line), and σ_- (dashed blue line) light. All were calculated with the same conditions as in Fig. 5. Note the logarithmic scale for both positive and negative spin currents. Lowercase letters indicate the transitions noted in Fig. 2. Since direct optical pumping and hyperfine-shift pumping have comparable rates but opposite signs at the transitions D_2(c–f), J_I changes sign as a function of detuning within each peak.

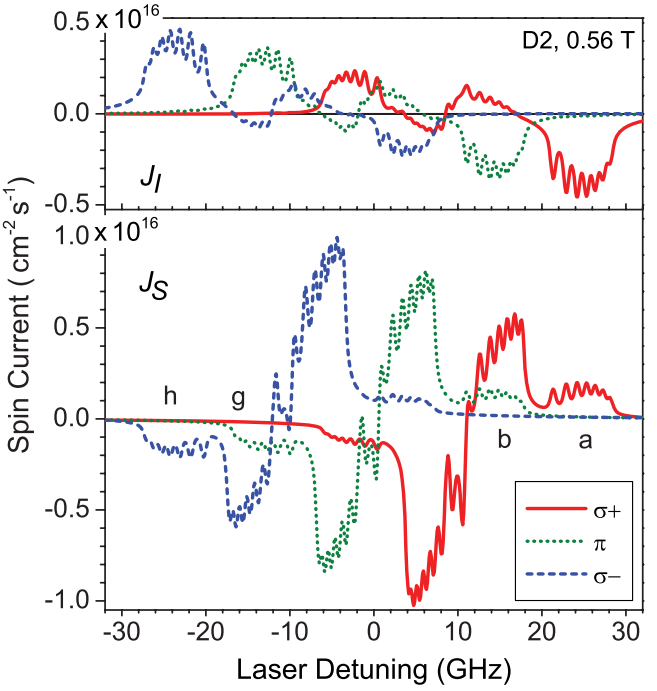

FIG. 7. (Color online) Simulated diffusion spin currents to the side wall of a cylindrical cell as a function of laser frequency across D_2 line at a magnetic field of 0.56 T, about 5 times smaller than the field of Fig. 5. Nuclear- and electron-spin currents J_I and J_S are induced by σ_+ (solid red line), π (dotted green line), and σ_- (dashed blue line) light. All were calculated by the same parameters as in Fig. 5, and plotted with a linear vertical scale. Many lines at small detuning overlap, so we only assign the labels of Fig. 2 to transitions that remain clearly defined at this lower field.

the mechanism for optical NMR enhancement. Despite three orders of magnitude difference in absorption cross section, the lines D_2(a), D_2(b), D_2(c), and D_2(e) produce similar magnitude J_I for σ_+ pumping.

Finally, we mention the currents for D_2 pumping at 0.56 T shown in Fig. 7. Because the Zeeman splitting is on the order of the hyperfine splitting, the current spectra are more asymmetric and overlap with each other. Nonetheless, the D_2(a) and D_2(h) lines are still well-resolved.

III. ALKALI SALT/VAPOR CELLS

For our experiments, crystallites of alkali salts, tiny droplets of Cs metal, and N_2 buffer gas were sealed inside cylindrical Pyrex glass cells. Most of the cells were manufactured at Princeton: flat optical windows were attached at both ends to allow better optical transmission, with a stem extending from the curved wall. Another set of cells, used at Hyogo, were closed at one end with a glass stem and at the other by a curved window. Cell preparation for this work has been described previously [13]. An *in situ* crystallite growth procedure was employed to maximize the surface area of the solid in contact with the vapor with the aim of optimizing spin transfer. We used NMR spectroscopy to detect only the Cs nuclei in the salt. The $\Delta m_S = 0$ NMR frequencies of Cs atoms in the vapor are detuned from those of the salt by ∼1 GHz at high fields due to the hyperfine interaction, and we do not observe them. The NMR frequency of Cs nuclei in metal droplets is detuned by a much smaller amount, about 1.45%, due to the Knight shift [24,25]. The ions in the glass have a very broad NMR resonance, and contribute an insignificant baseline to observed spectra.

IV. EXPERIMENTAL SETUP

The observations in this work were performed on two experimental setups—one at Princeton University and one at the University of Hyogo. In both setups, the pumping light was produced with a single-mode laser, and the general cell preparation procedure was the same. The magnetic field for the Princeton experiments (2.7 T and 9.4 T) was produced by a superconducting magnet, while the field (0.56 T) for the Hyogo experiments was produced by a permanent magnet. A schematic of the two setups is shown in Fig. 8. Each alkali-salt glass cell was placed in an NMR coil contained within an oven, and the assembly was inserted into the magnet. The oven was electrically heated to provide an adequate atomic number density. The magnetic fields produced by the heater were negligibly small.

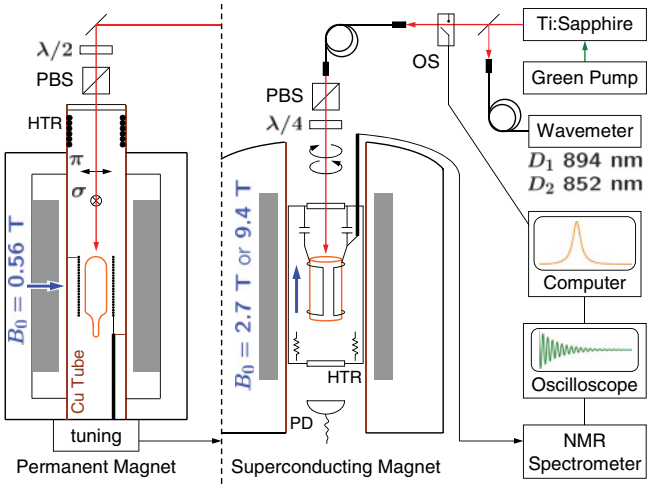

FIG. 8. (Color online) Experimental setup. Pump light from a cw Ti : sapphire laser was routed through an optical shutter (OS) and a multimode fiber into a superconducting magnet. The light was circularly polarized using a polarizing beamsplitter (PBS) and a quarter-wave ($\lambda/4$) plate, and uniformly illuminated a cylindrical cell. A photodiode (PD) was used to verify optical absorption prior to NMR experiments. A saddle-type coil sensed the free-induction-decay (FID) signals from the alkali-salt on the sidewall of the glass cell. The oven temperature was regulated by a resistive heater (HTR) and a proportional-integral-differential (PID) feedback controller. In the permanent magnet (left), the pump beam was perpendicular to the magnetic field, and linearly polarized with a PBS and a half-wave ($\lambda/2$) plate. The temperature of the magnet was regulated by chilled water to control drifts in the magnetic field. Low-frequency FID signals were picked up with a solenoid coil.

Once the cell temperature reached equilibrium, the Cs vapor in the cell was optically pumped with D_1 (894 nm) or D_2 (852 nm) light. A small fraction of the laser light was routed to a wavemeter to continuously monitor the laser frequency. At Princeton, a polarizing beamsplitter (PBS) cube and a $\lambda/4$ plate were placed in the beam path to provide $\sigma_\pm$ circularly polarized light. The laser beam was directed along the axis of the magnet and uniformly illuminated the cell at approximately 100 mW/cm^2. At Hyogo, the laser beam propagated perpendicularly to the magnetic field. A PBS and a $\lambda/2$ plate were adjusted to provide linearly polarized σ or π light illuminating the cell approximately at 1 W/cm^2. The magnetization of Cs nuclei in the salt was detected with a custom-made phase-sensitive NMR spectrometer. Each free induction decay (FID) following an excitation pulse was recorded and averaged on a digital oscilloscope, and Fourier transformed on a computer. The resonance peak for each FID was fit to a Gaussian, and the area underneath this fit was used as a measure of the Cs nuclear polarization. The procedure for acquiring thermal and pumped signals has been described elsewhere [13].

V. NMR ENHANCEMENT BY D_1 PUMPING

At the highest magnetic field available to us, 9.4 T, the absorption cross section for σ_+ light is largest for the transition D_1(a), and much smaller for the other transitions. Similarly, D_1(d) has the greatest absorption cross section for σ_- light. While optically pumping either of these two lines, the electron spin is directly polarized by depopulation pumping, and the nuclear spin is polarized in the same direction through the collisional hyperfine-shift interaction. Thus, the current J_I and J_S will have the same sign and similar line shapes near these resonances. These two lines can be pumped to produce large positive or negative enhancement, but there is no way to tell whether the enhancement is due to J_I and J_S, since both are expected to have the same sign.

At fields substantially lower than 9.4 T, the lines D_1(b, c) have absorption cross sections more comparable to those of D_1(a, d) since the energy basis states are further from the extreme high-field limit of uncoupled spin states that we discussed earlier. Optical pumping by $\sigma_\pm$ light on these transitions directly produces nuclear polarization in the Cs vapor that can be opposite the electron-spin polarization, and with a different line shape, as shown in Fig. 5. Measurements at low field can thus give more insight into the spin transfer mechanism to the salt. In the circle insets of Fig. 9, the NMR signals are shown for various pumping transitions. The NMR amplitude for transitions D_1(b, c) is roughly half that for transitions D_1(a, d), and is evident without averaging. The enhancements for D_1(b, c) changed sign when we changed the polarization of the light, indicating that the observed enhancement is due to J_I. As shown in Fig. 5, J_S is independent of polarization for these transitions, the only negative spin current at D_1(b) is J_I for σ_- light, and the only positive spin current at D_1(c) is J_I for σ_+ light. As listed in Table I, the polarizations achieved at 2.7 T (even at low temperature

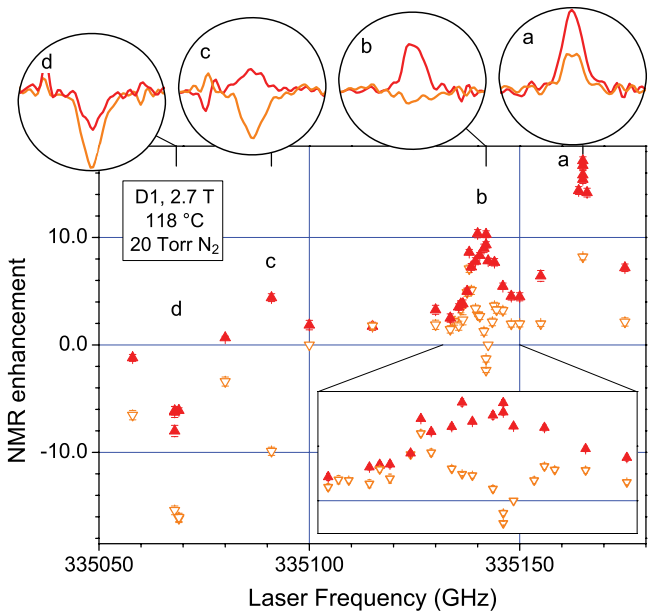

FIG. 9. (Color online) NMR enhancement at 2.7 T with 20 Torr N_2. The circle insets show NMR signals for σ_+ (red, gray) and σ_- (orange, light gray) pumping. The enhancement calculated from Gaussian fit to the thermal and enhanced NMR signals, depended on the polarization, σ_+ (red ▲) and σ_- (orange ▽). The pump laser frequency was scanned across the D_1 line. The box inset shows the fine structure near the D_1(b). Lowercase letters indicate the pump transition named in Fig. 2. The observed enhancement does not match any of the spin currents for pure pump light shown in Fig. 5.

TABLE I. Spin polarization of Cs nuclei in CsH for cells filled with N_2 gas of 20 Torr, 11 Torr, and 10 Torr. Enhancement ($E_i = A_i/A_{th}$, i = p or n) is from the NMR area of the thermal signal (A_{th}), the positively (A_p) or negatively (A_n) enhanced signal at the field B_0, and the D_1 or D_2 line. The enhanced polarization ($P_I = P_{th}E_i$) is calculated for $|E_i| > |E_{j\neq i}|$ and the polarization $P_{th} = \langle I_z\rangle/I = h\nu_0(I+1)/3k_BT$ at the thermal equilibrium and the NMR frequency of ν_0.

B_0 (T)	N_2 (Torr)	Line	T (°C)	E_p	E_n	P_I (ppm)
9.4	11	D_1	137	3.8	−4.3	−40
	20	D_1	135	2.9	−1.8	27
2.7	20	D_1	118	17.1	−16.2	48
	10	D_1	96	8.0	−7.6	23
	10	D_2	108	15.0	−15.3	−44

for a cell with 20 Torr N_2) were greater than those achieved at 9.4 T.

We tuned the pump laser frequency over a range including all four D_1 transitions, and the resulting NMR enhancements in the salt are shown in Fig. 9. Surprisingly, the spectrum exhibited fine structure near the transition D_1(b), as shown in the box inset—a narrow negative-enhancement feature occurs within a broader positive bump. This feature, along with positive enhancement for σ_- light at D_1(a) and negative enhancement for σ_+ light at D_1(d), suggests that the polarization of the pump light is significantly mixed by the vapor.

Most spectroscopic measurements of the vapor are more weighted toward the middle of the cell, but our NMR measurements are more strongly influenced by the atoms near the cell walls. To understand the mechanism of spin transfer to salts, we must therefore consider the possibility of strong absorption and emission near the wall, as shown in Fig. 10. In a 10 Torr N_2 cell, roughly 20% of the excited atoms decay by spontaneous emission [26], producing unpolarized light that will propagate in all directions and evenly illuminate the walls. The pump beam is strongly attenuated near the walls, so atoms in the back half of the cell will be significantly pumped by the

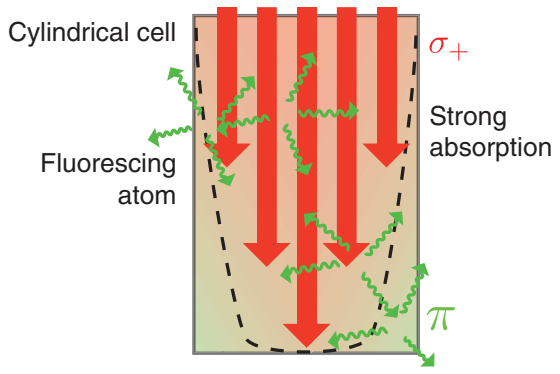

FIG. 10. (Color online) Schematic of a mechanism for polarization mixing in alkali vapors at high magnetic field. For pumping on the transition D_1(a) with σ_+ light, the unpolarized vapor near the walls absorbs and strongly attenuates the pump light, leading to a strongly fluorescing layer near the cell walls. Fluorescent light with π polarization is more likely to be emitted toward the sidewall, where it will be reabsorbed by the vapor.

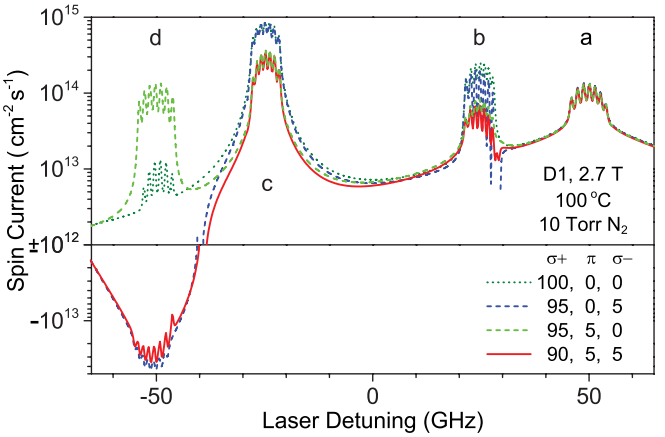

FIG. 11. (Color online) The nuclear-spin current J_I simulated for partially polarized D_1 light. The relative power of each polarization is shown as a percentage. Our simulations ignore the propagation direction of the light; the π polarized light is mixed in as a simple model for fluorescence. The parameters for calculation are the same as those in Fig. 5. The solid red curve can be compared to the enhanced signals (red ▲ in Fig. 9). Note the logarithmic vertical scale.

fluorescent light. This mechanism can produce much more polarization mixing than we would expect from distortions and birefringence in our optics or from stray unpolarized light.

As a simple approximation for light polarization mixing due to both internal and external mechanisms, we simulated J_I for various impure polarizations, as shown in Fig. 11. In our simulations, the frequency of each light polarization was the same, but in a real cell, the fluorescent light polarization and intensity depends on the details of deexcitation in the atomic vapor. In the case of D_1(b) pumping with σ_+ light, for example, the strongest fluorescence will have π polarization (see Fig. 4). The most striking effect of polarization mixing is the reversal of the simulated sign of J_I for transition D_1(d) for even a small amount of σ_- light. The relative amplitudes of J_I for D_1(a) and D_1(b) are reversed for a small amount of π light mixed in. Both of these simulation results are consistent with the observed amplitude of enhancement spectra in Fig. 9, though the observed enhancement for D_1(c) is much smaller than predicted. The general agreement between our simulations and experimental data indicate that the observed enhancement is due to J_I induced by polarization-mixed light.

The current J_I is not, however, simply a sum of currents induced by pumping with pure light of different polarizations. The absorption cross section for σ_- light is much greater than that for π light at D_1(d), and will have a correspondingly greater effect on the spin currents. Light with σ_- polarization will also be more strongly attenuated as it passes through the vapor; we expect the agreement between simulations and experiments to improve once we take into account light intensity inhomogeneities [27]. Since σ_+ light is significantly absorbed at D_1(c), σ_+ pumping leads to π fluorescence at D_1(c) and σ_+ fluorescence at D_1(a). The nuclear-spin currents induced by these two polarizations of fluorescent light have opposite sign, which would result in smaller NMR enhancements than our simulations predict. A similar situation arises for σ_- pumping at D_1(b).

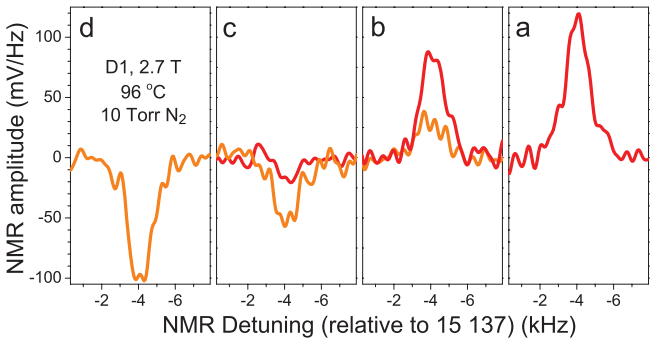

FIG. 12. (Color online) NMR signals at 2.7 T for the cell with 10 Torr N_2, were enhanced at four D_1 lines with σ_+ (red, gray) and σ_- (orange, light gray) lights. In contrast to the signals with 20 Torr N_2 in Fig. 9, the sign was unchanged by switching the pump polarization at D_1(b) and D_1(c).

We also measured the NMR enhancement in a cell with only 10 Torr N_2 buffer gas, and found that the enhancement due to pumping on D_1(a, b) was positive, while the enhancement for D_1(c, d) was negative, independent of the pump polarization, as shown in Fig. 12. This reduced dependence on pump polarization arose because, at lower buffer-gas pressures, deexcitation due to fluorescence has a stronger effect, leading to stronger polarization mixing.

VI. NMR ENHANCEMENT BY D_2 PUMPING

We further investigated NMR enhancement due to D_2 pumping. Because of the large Zeeman splitting, D_2 transitions are resolved even in buffer-gas cells at high field. Figure 13 shows the enhancement for six D_2 transitions for both σ_+ and σ_- polarized pump light in a cell with 10 Torr N_2. Four allowed transitions, D_2(b, c) for σ_+ light, and D_2(f, g) for σ_- light,

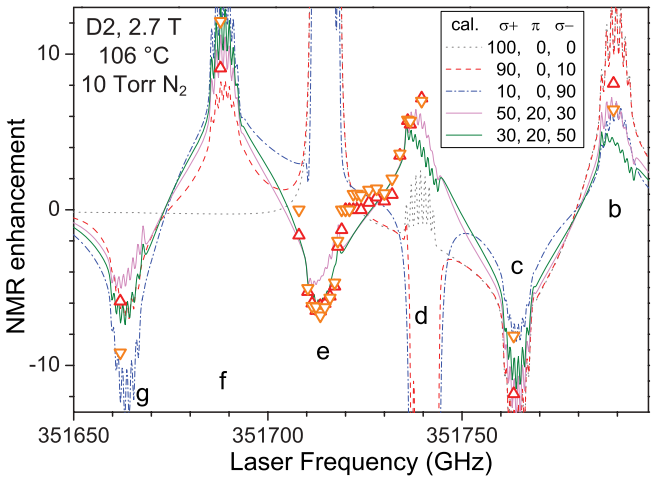

FIG. 13. (Color online) Enhancement measured by D_2 pumping at 2.7 T with 10 Torr N_2. Weak dependence on pump polarization, σ_+ (red △) or σ_- (orange ▽), was observed. Lowercase letters denote the transitions named in Fig. 2. The curves are J_I calculated for partially polarized light, again, including π polarized light as a simple model for fluorescence. The relative power of each polarization is shown as a percentage. The mixed-polarization spin currents are not linear combinations of the pure-polarization spin currents of Fig. 6.

presented a weak but clear dependence on pump polarization. This weak dependence is consistent with the cell's weak dependence on polarization for D_1 pumping. The sign of the observed signals is, nevertheless, consistent with J_I calculated for the allowed transitions of $\sigma_\pm$ light, respectively, as shown in Fig. 6. The NMR enhancement due to pumping on σ_+ and σ_- light at the forbidden transitions D_2(d, e) was independent of pump polarization, and both had the same dependence on frequency. Since the sign of J_I is opposite for direct σ_+ and σ_- pumping at these transitions, and since the peaks in J_I are offset by 1.2 GHz from each other, the observed enhancement must be due to J_I induced by fluorescent π polarized light.

We simulated the nuclear-spin current J_I, accounting for fluorescent light by artificially introducing polarization mixing in the pump light. The blue (dashed-dot) and red (dashed) curves show simulated J_I for slightly mixed σ light, and they closely match the observed enhancement for the four allowed transitions D_2(b, c, f, g), but predict the wrong sign of enhancement for the forbidden transitions D_2(d, e). By including π polarized light, our simulations match the observed enhancement, again indicating that the light polarization is strongly mixed near the cell walls. Further simulations taking into account the spatial distribution and the full optical frequency spectrum of the fluorescent light will help to confirm this interpretation.

Because the polarization of pump beam was noncritical, unpolarized light was used for D_2 pumping shown in Fig. 14. By removing the polarizing optics, we also increased the pump intensity. As indicated in Table I, the spin polarization from D_2 pumping is greater than that from D_1 pumping at 2.7 T for the 10 Torr cell. Since the efficiency of spin transfer from the vapor to the solid remained unchanged, this difference indicates that greater spin currents were induced by D_2 pumping.

A unique advantage of D_2 pumping is the presence of the forbidden transition D_2(a), which produces $J_S > 0$ and $J_I < 0$ for σ_+ light, and negligible currents from other polarizations, as shown in Fig. 6. In Fig. 14, we show NMR enhancement due to pumping on the transition D_2(a), as well as the allowed

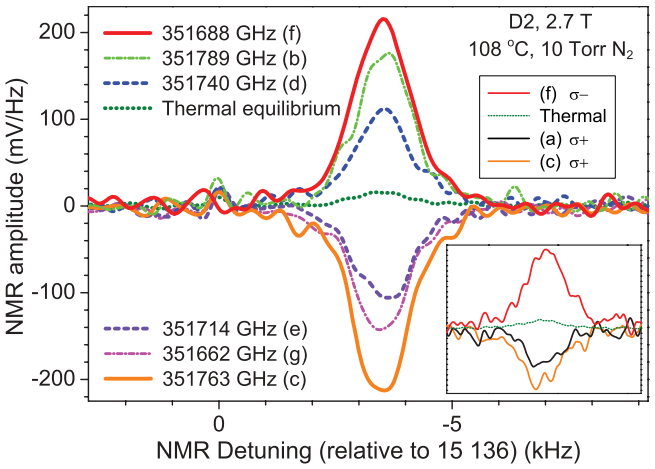

FIG. 14. (Color online) Cs NMR signals of hydride in the 10 Torr cell at 2.7 T were enhanced by unpolarized light at six D_2 lines. The inset shows negative enhancement from polarized light at D_2(a) (black curve). The signal amplitude was degraded because these were recorded half a year later after the unpolarized pump measurements.

transitions D_2(c, f) for comparison. The enhancement due to D_2(a) pumping is negative, again indicating that NMR enhancement is due to J_I induced in the vapor. Since $J_S \approx 100\, J_I$ for the allowed transitions, which show comparable enhancement to D_2(a), the contribution of J_S to the NMR enhancement must be small.

VII. INTERMEDIATE MAGNETIC FIELD

At an intermediate field, 0.56 T, the thermal NMR signal of the CsH was smaller than our detector noise, so we adjusted the phase of our NMR detection using a large amount of CsCl immediately before optical pumping experiments—positive signals indicate polarization parallel to the thermal polarization in the CsCl. Without knowing the thermal signal, we cannot calculate an enhancement E_i, but we can compare the enhanced signals.

As shown in Fig. 7, several spin current peaks overlap for small detunings of the D_2 pump. We measured enhanced NMR signals of CsH undergoing optical pumping with σ polarized light propagating perpendicular to the magnetic field; the results are shown in Fig. 15. In agreement with simulated J_I for $\sigma_\pm$ polarized pumping in a cell with 10 Torr N_2 buffer gas, we observed negative and positive enhancement, respectively, for detunings of +5 GHz and −5 GHz [see Fig. 15(a)]. We observed no significant enhancement from π pumping at ±5 GHz.

We also measured the enhanced NMR signal in a cell with no buffer gas. As shown in Fig. 15(b), the enhanced signals have opposite sign from those in the gas cell. Under the conditions of our experiment ($P_L = 0.5$ W/cm^2, $\sigma_{op} \approx 10^{-12}$ cm^2), the mean optical pumping time, $1/\Gamma_{op} \approx 1\mu$s, is shorter than the mean time between wall collisions, $\tau_w \approx 40\mu$s, which is in turn shorter than the mean time between collisions with residual gases. Thus, the unpolarized atoms leaving the wall will easily be optically pumped before reaching another wall. We can then express the nuclear-spin current density as

$$J_I = [\mathrm{Cs}] \int_0^\infty \langle I_z \rangle v f(v)\, dv\,, \tag{6}$$

where $f(v)$ is a velocity distribution function, and the positive integration region indicates current toward the wall. For our cylindrical cells, we can neglect the velocity dependence of relaxation [28], and as long as the pump power is sufficient to produce polarization across the entire velocity distribution, we have $J_I \propto \langle I_z \rangle$.

The opposite signs for enhancement in the vacuum cell and the buffer-gas cell arose because of the relative contributions of quenching and spontaneous emission in the vapor. For example, at −5 GHz detuning [corresponding roughly to the high-field transition D_2(f)], the pump light excites the transitions $|m_S = -1/2, m_I\rangle \rightarrow |m_J = -3/2, m_I\rangle$, as shown in Fig. 16. Due to the hyperfine interaction, the states labeled $|m_S = -1/2, m_I\rangle$ are mixtures of states,

$$|I, m_I\rangle \otimes |S, -1/2\rangle - \epsilon |I, m_I - 1\rangle \otimes |S, +1/2\rangle\,,$$

where $\epsilon = \delta\sqrt{(I + m_I)(I - m_I + 1)} \sim 0.2$ at 0.56 T. The mixing in the excited state is much smaller, with $\epsilon' \sim 0.005$. Due to this ground-state mixing, the pump transition will

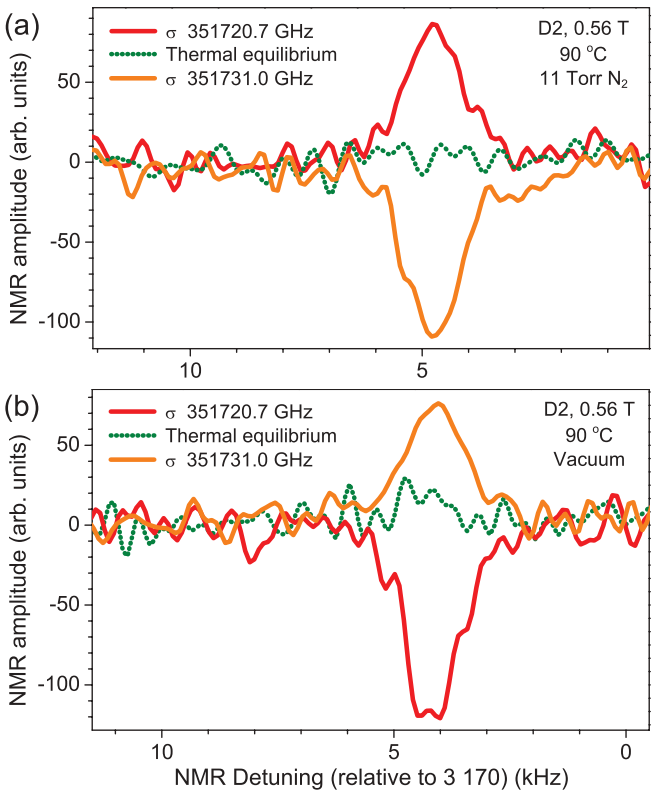

FIG. 15. (Color online) Cs NMR signals of hydride were enhanced at 0.56 T by linearly polarized σ light of D_2 line in cells (a) 11 Torr N_2 and (b) no buffer gas. The thermal signal was below the noise level (dotted green line). Each spectrum is a Fourier transform after averaging 70 FID's. RF pulses at a tipping angle of $\pi/3$ were applied at a repetition period of 100 s. Note the spin polarization oppositely enhanced for these cells at respective laser frequencies. The NMR frequency was shifted for these cells because of the difference in cell position and the drift of magnetic field.

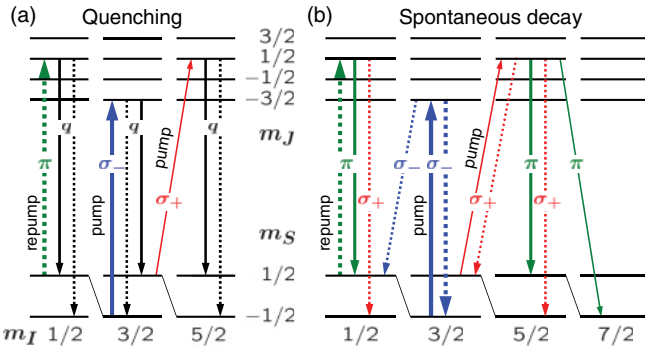

FIG. 16. (Color online) $\langle I_z \rangle$ for σ pumping and the contribution of (a) quenching (black) and (b) spontaneous decay on σ_+ (red), π (green), σ_- (blue) transitions. A single laser works as pump and repump due to overlapping of lines and mixing of π light. Especially when pumping from $|m_S, m_I\rangle = |-1/2, 3/2\rangle$, the repump transitions are very close to the pump transitions at −5 GHz. $\langle I_z \rangle$ increases (solid arrow) and decreases (dotted arrow) in each process. Thickness of the arrows indicates the transition strength. Each of the arrows represents transitions for several sublevels with different m_I.

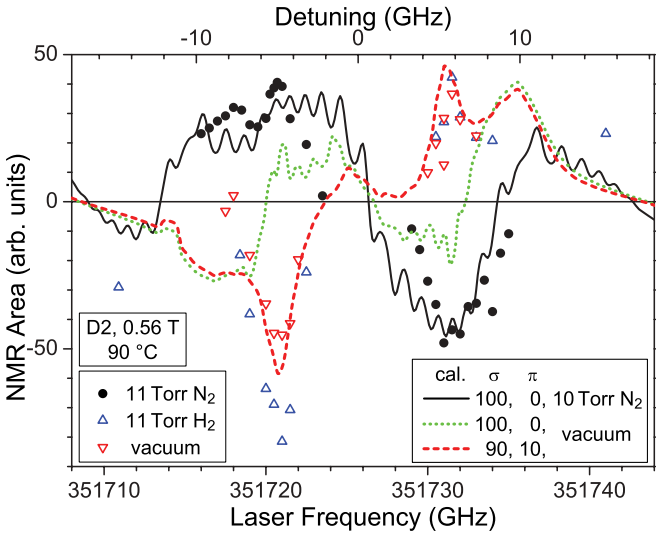

FIG. 17. (Color online) NMR area at 0.56 T enhanced by D_2 pumping with σ light in the hydride cells filled with 11 Torr N_2 (•), 11 Torr H_2 (blue △), and no buffer gas (red ▽). The solid black curve shows the sum of J_I for $\sigma_\pm$ polarizations in Fig. 7. For the vacuum cell, $\langle I_z \rangle$ is calculated for pure σ light (dotted green) and partially polarized light (dashed red).

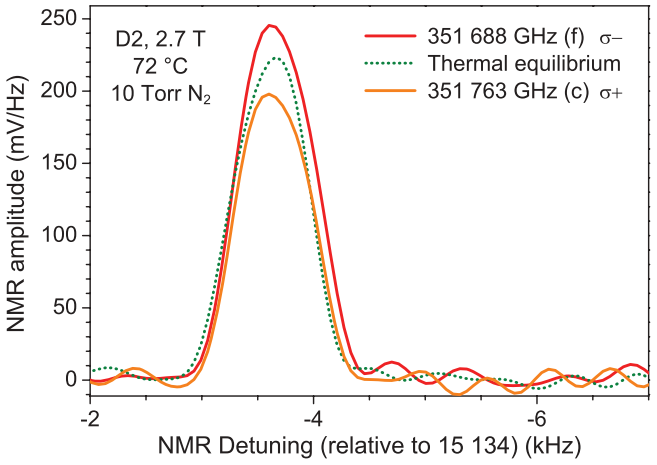

FIG. 18. (Color online) Single-shot NMR signal of CsCl for accumulation time of 30 min, 10 Torr N_2, 2.7 T, and 72 °C. The difference between the amplitudes for σ_+ and σ_- pumping is on the same order as those of CsH signals shown in Fig. 14.

increase the nuclear spin by ϵ^2. When quenching dominates the deexcitation, as in the gas cell, the nuclear spin is conserved, while the electron spin is randomized, leading to a net gain of nuclear spin during an optical pumping cycle [see Fig. 16(a)].

On the other hand, if spontaneous emission dominates the deexcitation, as in the vacuum cell, the excited atoms can decay along the σ_- (dotted blue) transitions indicated in Fig. 16(b). The strongest of these transitions is back to the original ground state, which induces no net change in the nuclear spin. However, the other transition decays to the state $|I,1/2\rangle \otimes |S,+1/2\rangle + \epsilon|I,3/2\rangle \otimes |S,-1/2\rangle$, inducing a net loss of nuclear spin. At these fields, the pump beam is resonant with more than one transition, and can serve as a repumping beam, so there is no significant difference between the electron-spin polarization in these two cases.

We measured three types of cells at 0.56 T: cells filled with 11 Torr N_2 gas, with 11 Torr H_2 gas, and with no buffer gas. The enhanced NMR signals as functions of pump laser detuning are shown in Fig. 17. The enhanced NMR signals in the N_2 cells agree well with our simulated J_I for σ light, and the enhanced NMR signals for both H_2 and vacuum cells agree well with simulated $\langle I_z \rangle$ assuming weak polarization mixing of the pump light. The similarity between the H_2 cell and the vacuum cell indicate that the H_2 gas had reacted with excess Cs in the vapor cell to form more CsH salt, reducing the buffer-gas pressure essentially to zero. Similar to the high-field case, we found that the observed NMR signals did not match the electron-spin current J_S nor the electron-spin polarization $\langle S_z \rangle$, so the polarization in the salt is mostly due to nuclear-spin currents in the vapor.

VIII. SPIN TRANSFER TO A STABLE SALT

We also measured the enhancement of the NMR signal for the stable salt CsCl in contact with an optically pumped Cs vapor. Since CsCl is stable, we did not need to form crystallites *in situ* as we did with CsH. Instead, we melted a large amount of commercial CsCl crystals in a cell under atmosphere to coat the sidewall, then attached the cell to a vacuum manifold to add Cs metal and buffer gas. This procedure resulted in a much larger thermal NMR signal as seen in Fig. 18. As before, we optically pumped the vapor on the transitions D_2(c) and D_2(f) at 2.7 T to achieve maximum spin currents.

We found that the change in the integrated NMR signal was comparable to that in the CsH cells. Since the longitudinal relaxation time for Cs in CsCl is longer than in CsH, we expected the enhancement to be greater; the observed enhancements indicate that the transfer of polarization to the salt may be limited by its surface area in contact with the vapor coating with thick salt of a smooth surface could be improved.

Cesium hydride is dissociative at the temperature of our experiments [29]; at equilibrium for the chemical reaction $2CsH \rightleftharpoons 2Cs + H_2$, the pressure of H_2 gas is about 10^{-3} Torr at 130 °C [30]. For this reason, we initially suspected that the salt polarization was due to replacement of Cs ions by polarized Cs atoms. However, CsCl is stable (melting point 646 °C, boiling point 1290 °C) and the pressure of Cl_2 gas is negligibly small at 130 °C [30]. Since the NMR enhancement for both salts was comparable, ion replacement did not play a significant role in the spin transfer process from the vapor to the salt, so nuclear dipole interactions are the most likely mechanism for transfer. Moreover, we showed that spin transfer is not limited to CsH, and can be applied to other salts.

IX. TEMPERATURE LIMIT

An easy way to increase the spin current to the cell walls is to increase the Cs number density by raising the cell temperature, since $J_I \propto$ [Cs] as long as the optical pumping rate is high enough. By contrast, the relaxation time for Cs nuclear polarization in the salt decreases upon heating [12]. We measured the NMR enhancement in a cell with CsH over a range of temperatures at 9.4 T to try to optimize the enhancement; the results are shown in Fig. 19. We found that

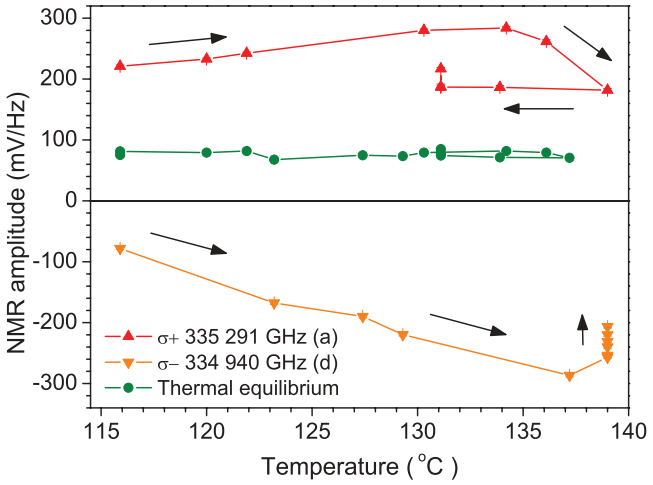

FIG. 19. (Color online) Temperature dependence and time sequence of NMR amplitude for the 11 Torr cell at 9.4 T. The positive signal (red ▲) was induced by σ_+ light at D_1(a) and the negative (orange ▼) by σ_- light at D_1(d). The thermal amplitude (green •) was almost constant. The temperature was first increased as indicated by the arrows, then decreased because the signal was depleted. After decreasing, the enhancement in this cell never returned to its previous maximum.

the enhancement due to pumping on transitions D_1(a) and D_1(d) was equal in magnitude at lower temperatures (116 °C), but the negative enhancement due to D_1(d) pumping grew faster with temperature.

We also found for unknown reasons that the enhancement for both pump transitions rapidly decreased above 135 °C, and remained at a reduced value when returned to lower temperatures. Since the thermal NMR signal remained constant, the amount of salt did not change; heating induced some unknown change in the CsH crystal that reduced its potential for NMR enhancement. For this reason, all other measurements at 2.7 T and 0.56 T were performed at temperatures lower than 120 °C.

X. SUMMARY

We have demonstrated enhancement of the Cs NMR signal in salts due to optical pumping of Cs vapor at various magnetic fields. By pumping with a variety of D_1 and D_2 lines, we induced electronic- and nuclear-spin currents with various magnitudes and different signs. Comparing observed enhancements to simulated spin currents, we found that the nuclear-spin current was the dominant source of Cs nuclear polarization in the salt. We also showed that light polarization mixing near the cell walls contributes significantly to the observed enhancement. Laser-induced spin currents also enhanced the NMR signal in the stable salt CsCl, ruling out ion replacement as a spin transfer mechanism and demonstrating the potential for spin polarizing a variety of materials.

ACKNOWLEDGMENTS

The authors would like to thank M. Souza for his advice and glassblowing skills, and S. Parameswaran for his support on the experiment. This work was partially supported by the Air Force Office of Scientific Research and the Grant-in-Aid for Scientific Research of JSPS and MEXT. K.I. is grateful for the support and opportunities provided by Princeton University and the University of Hyogo.

[1] A. Wolber *et al.*, Nucl. Instrum. Methods Phys. Res., Sect. A **526**, 173 (2004).
[2] A. E. Dementyev, D. G. Cory, and C. Ramanathan, Phys. Rev. Lett. **100**, 127601 (2008).
[3] A. K. Paravastu, S. E. Hayes, B. E. Schwickert, L. N. Dinh, M. Balooch, and J. A. Reimer, Phys. Rev. B **69**, 075203 (2004).
[4] B. M. Goodson, *Applications of Optical Pumping and Polarization Techniques in NMR* (Elsevier Scientific, New York, 2005), Vol. 55
[5] J. Ball, Nucl. Instrum. Methods Phys. Res., Sect. A **526**, 7 (2004).
[6] T. G. Walker and W. Happer, Rev. Mod. Phys. **69**, 629 (1997).
[7] N. D. Bhaskar, J. Camparo, M. Ligare, and W. Happer, Phys. Rev. Lett. **46**, 1387 (1981).
[8] T. Rõõm, S. Appelt, R. Seydoux, E. L. Hahn, and A. Pines, Phys. Rev. B **55**, 11604 (1997).
[9] R. W. Adams, J. Aguilar, K. D. Atkinson, M. J. Cowley, P. I. P. Elliott, S. B. Duckett, G. R. Green, I. G. Khazal, J. López-Serrano, and D. C. Williamson, Science **323**, 1708 (2009).
[10] E. G. Wikner, W. E. Blumberg, and E. L. Hahn, Phys. Rev. **118**, 631 (1960).
[11] B. T. Saam, Ph.D. thesis, Princeton University, 1995.
[12] B. Patton, Ph.D. thesis, Princeton University, 2007 [http://www.princeton.edu/physics/academics/graduate-program/theses/theses-from-2007/].
[13] K. Ishikawa, B. Patton, Y. Y. Jau, and W. Happer, Phys. Rev. Lett. **98**, 183004 (2007).
[14] W. Happer, Y.-Y. Jau, and T. G. Walker, *Optically Pumped Atoms* (Wiley-VCH, Weinheim, 2010).
[15] W. Happer, Rev. Mod. Phys. **44**, 169 (1972).
[16] W. Happer, *High Field Diffusion* (internal note, 2006).
[17] N. Beverini, P. Minguzzi, and F. Strumia, Phys. Rev. A **5**, 993 (1972).
[18] S. Appelt, A. B.-A. Baranga, C. J. Erickson, M. V. Romalis, A. R. Young, and W. Happer, Phys. Rev. A **58**, 1412 (1998).
[19] D. K. Walter, W. M. Griffith, and W. Happer, Phys. Rev. Lett. **88**, 093004 (2002).
[20] M. Arditi and T. R. Carver, Phys. Rev. **124**, 800 (1961).
[21] P. J. Oreto, Y.-Y. Jau, A. B. Post, N. N. Kuzma, and W. Happer, Phys. Rev. A **69**, 042716 (2004).
[22] W. Happer, *High-Field Optical Pumping* (internal note, 2006).

[23] F. Masnou-Seeuws and M. Bouchiat, J. Phys. (France) **28**, 406 (1967).
[24] C. H. Townes, C. Herring, and W. D. Knight, Phys. Rev. **77**, 852 (1950).
[25] B. Patton, K. Ishikawa, Y.-Y. Jau, and W. Happer, Phys. Rev. Lett. **99**, 027601 (2007).
[26] D. A. McGillis and L. Krause, Can. J. Phys. **46**, 1051 (1968).
[27] B. A. Olsen, Ph.D. thesis, Princeton University, 2011 [http://www.princeton.edu/physics/academics/graduate-program/theses/theses-from-2011-1/].
[28] K. Ishikawa, K. Iida, and T. Nakura, Phys. Rev. A **63**, 013405 (2000).
[29] F. R. Brown and W. Happer, Phys. Lett. A **94**, 81 (1983).
[30] T. B. Reed, *Free Energy of Formation of Binary Compounds* (MIT Press, Boston, 1971).